Biomed Microdevices (2016) 18: 49
DOI 10.1007/s10544-016-0068-9

3D printing enables separation of orthogonal functions within a hydrogel particle

Ritu Raman[1,2] · **Nicholas E. Clay**[3] · **Sanjeet Sen**[3] · **Molly Melhem**[4] · **Ellen Qin**[3] · **Hyunjoon Kong**[3] · **Rashid Bashir**[2,4]

Published online: 23 May 2016

Abstract Multifunctional particles with distinct physiochemical phases are required by a variety of applications in biomedical engineering, such as diagnostic imaging and targeted drug delivery. This motivates the development of a repeatable, efficient, and customizable approach to manufacturing particles with spatially segregated bioactive moieties. This study demonstrates a stereolithographic 3D printing approach for designing and fabricating large arrays of biphasic poly (ethylene glycol) diacrylate (PEGDA) gel particles. The fabrication parameters governing the physical and biochemical properties of multi-layered particles are thoroughly investigated, yielding a readily tunable approach to manufacturing customizable arrays of multifunctional particles. The advantage in spatially organizing functional epitopes is examined by loading superparamagnetic iron oxide nanoparticles (SPIONs) and bovine serum albumin (BSA) in separate layers of biphasic PEGDA gel particles and examining SPION-induced magnetic resonance (MR) contrast and BSA-release kinetics. Particles with spatial segregation of functional moieties have demonstrably higher MR contrast and BSA release. Overall, this study will contribute significant knowledge to the preparation of multifunctional particles for use as biomedical tools.

Keywords Hydrogel · Polyethylene glycol · Stereolithography · 3D printing · Biomaterial

Ritu Raman and Nicholas Clay contributed equally to this work.

Electronic supplementary material The online version of this article (doi:10.1007/s10544-016-0068-9) contains supplementary material, which is available to authorized users.

✉ Rashid Bashir
rbashir@illinois.edu

[1] Department of Mechanical Science and Engineering, University of Illinois at Urbana-Champaign, 1206 West Green Street, Urbana, IL 61801, USA

[2] Micro and Nanotechnology Laboratory, University of Illinois at Urbana-Champaign, 208 North Wright Street, Urbana, IL 61801, USA

[3] Department of Chemical and Biomolecular Engineering, University of Illinois at Urbana-Champaign, 600 South Mathews Avenue, Urbana, IL 61801, USA

[4] Department of Bioengineering, University of Illinois at Urbana-Champaign, 1270 Digital Computer Laboratory, MC-278, 1304 West Springfield Avenue, Urbana, IL 61801, USA

1 Introduction

In recent years, an increasing number of multifunctional particle formulations have been developed for a variety of applications, ranging from consumer products to drug delivery devices (Bhaskar et al. 2010). Incorporating multiple functionalities into a single particle significantly reduces the total number of particles needed for any given application, as in the case of theranostic (dual therapeutic and diagnostic) nano- and micro-particles (Yang et al. 2012). Moreover, spatial separation of dual functionalities in a single particle may enable a synergistic physical or chemical property that cannot be replicated by two single-functional particles in the same dispersion (Shevchenko et al. 2008). This motivates developing a fabrication methodology for assembly of multiphasic particles, in which different functional modalities are spatially separated to avoid interference between them. A series of fabrication strategies have been proposed to prepare multiphasic particles, such as electrojetting, emulsification, and standard lithography techniques (Roh et al. 2005; Shah et al. 2009; Li et al. 2016). Despite impressive results reported to date, concerns still remain regarding the customizability of these techniques.

A wide variety of 3D printing technologies and printable biomaterials have been developed to suit the needs of biomedical applications (Melchels et al. 2010; Raman and Bashir 2015). Of these materials, highly absorbent hydrogels have been of particular interest to the biomedical community due to their tuneable stiffness and permeability. Hydrogels can be functionalized with various bioactive moieties by chemical modification of gel-forming polymers (Peppas et al. 2006; Arcaute et al. 2011). Taking advantage of the rapid development of this field, this study demonstrates a 3D printing-based strategy to manufacture biphasic hydrogel particles with spatially distributed functional moieties. Specifically, a stereolithographic apparatus (SLA) was used to fabricate hydrogel particles with distinct functional compartments. Using this fabrication technology, we examined whether controlling laser irradiation speed, which in turn allows for tuning of the energy dose delivered to pre-gel solutions, could be used to predict and control the cross-linking kinetics of the radical polymerization reaction. By doing so, we were able to customize and control the shape, size, and aspect ratio of the layers of the gel particles with great precision. We tested boundary stability across different layers using brightfield and confocal microscopy, and used these results to incorporate two moieties, bovine serum albumin (BSA) and superparamagnetic iron oxide nanoparticles (SPIONs), into biphasic gel particles. The release kinetics of BSA and magnetic resonance imaging (MRI) contrast of particles were evaluated to test the effect of spatially segregating orthogonal functions within a particle. The results of this study demonstrate an expedited approach for assembling multifunctional bioactive gel particles for a diverse array of biomedical applications including image-based targeted drug delivery.

2 Results and discussion

2.1 3D printing of hydrogel particle arrays

A commercial SLA was modified for printing photosensitive hydrogel polymers as previously demonstrated and shown in Fig. 1a (Chan et al. 2010). Liquid pre-gel solution, composed of poly (ethylene glycol) diacrylate (PEGDA) and a biocompatible photo-initiator, was injected onto the motorized stage and selectively cured by the SLA's ultraviolet laser. Following fabrication of each layer, the motorized stage moved down by a prescribed amount, and a new layer of pre-gel solution was manually injected and subsequently polymerized.

To enable high-throughput fabrication of many gel particles, the computer-controlled laser traced a 2D cross-section of the 3D hydrogels prescribed by a computer aided design (CAD) file, shown in Fig. 1b. This file contained a 30 × 30 array of cylinders of specified diameter and spacing. Due to the swelling properties of the hydrogels used in this study, these CAD-prescribed dimensions were not preserved in the final fabricated part. Figure 1b shows that an array of PEGDA 700 g mol^{-1} cylinders 200 μm in diameter spaced 200 μm apart becomes, after immersion and swelling in a solution of phosphate buffered saline (PBS) for an hour, an array of cylinders 270 μm in diameter spaced 130 μm apart. This trend was preserved for gel cylinders of larger diameters, as demonstrated in Figs. 1c-d and Fig. S1a, with gel arrays demonstrating an average swelling ratio of 140 %. This result is consistent with results previously demonstrated for polymerization of PEGDA hydrogels (Neiman et al. 2015; Raman et al. 2015).

The ultraviolet illumination energy dose required to cure photosensitive polymer solutions has been previously characterized by the cure-depth equation (Bartolo 2011; Stampfl and Liska 2011), an adapted form of the Beer-Lambert equation which relates the intensity of a light source to the exponential decay of its intensity in an absorbing medium. The SLA regulates ultraviolet light intensity by keeping the laser power constant (23 mW cm^{-2}) and adjusting laser scan speed to regulate the energy density delivered (ranging from 108 to 266 mJ cm^{-2} in this study).

The effect of ultraviolet light density on pre-gel solutions of PEGDA (400 g mol^{-1} and 700 g mol^{-1}) was tested, revealing that the degree of cross-linking was directly dependent on the energy dose delivered to the PEGDA, as shown in Fig. 2a. The thickness of the gels was likewise regulated by tuning the energy dose, as shown in Fig. 2b and Fig. S1b. Gel thickness was also shown to be dependent on the concentration of PEGDA in the pre-gel solution (20 % and 30 % PEGDA 700 g mol^{-1}), with increasing concentration correlated with increasing thickness, as demonstrated in Fig. 2c.

2.2 Fabrication of multi-layered hydrogel particles

The ability of the SLA to precisely tune the diameter, thickness, and spacing of gel arrays provided a highly reproducible methodology with which to fabricate multi-layered gel particles. The dimensions and properties of each layer could be tuned by regulating the composition of the pre-gel solution used in each layer. For instance, solutions of PEGDA 700 g mol^{-1} prepared with different fluorescent dyes (i.e., red-colored rhodamine and green-colored fluorescein) were used to study the spatial separation and boundary stability of multi-layer gel particles via confocal imaging. Specifically, a confocal microscope was used to measure the fluorescence intensity (represented by gray value) emitted by the gels in response to illumination at two different excitation wavelengths. Plots of measured mean gray value as a function of position along the thickness of two-layer, three- layer, and four-layer gels are

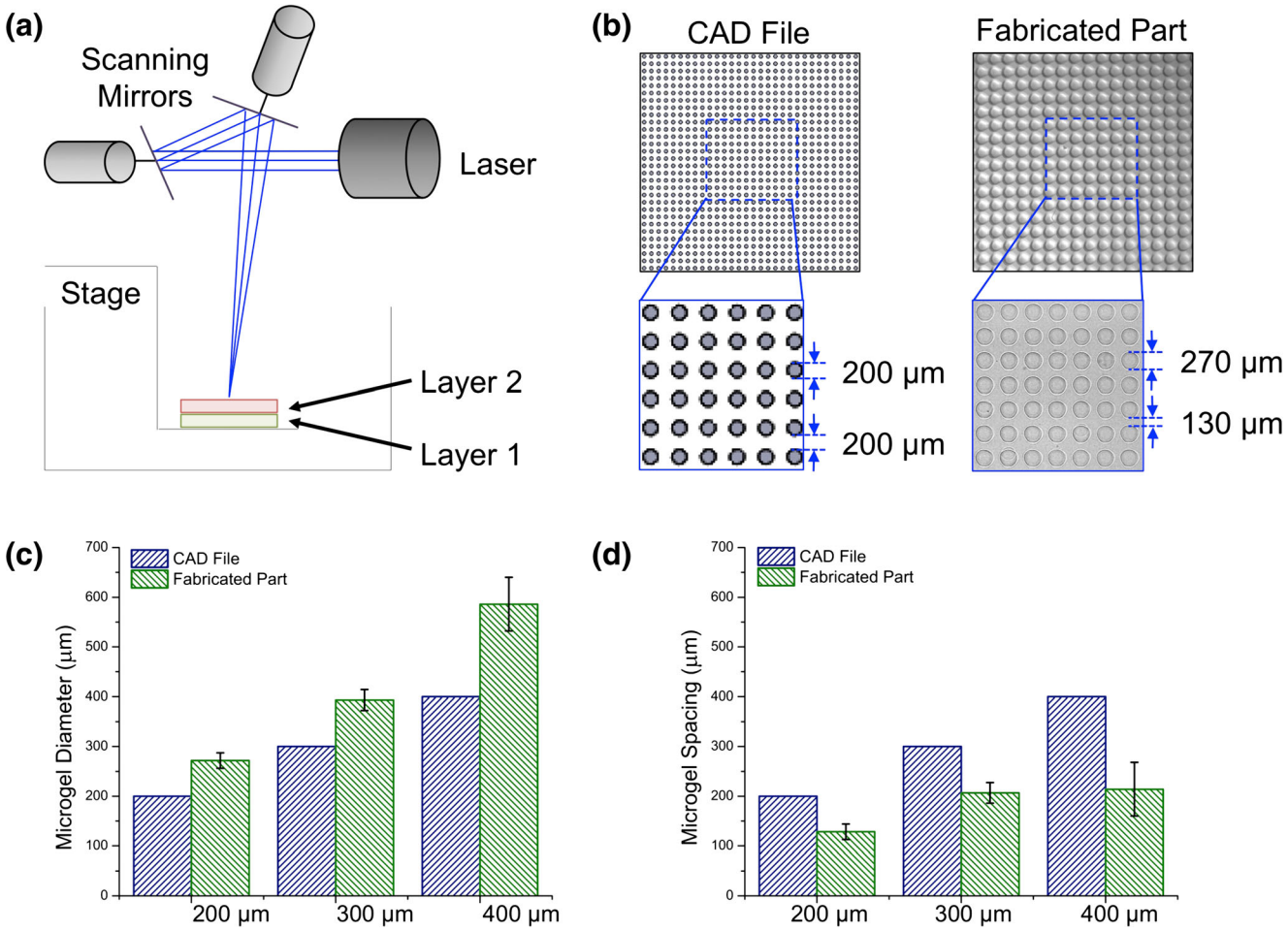

Fig. 1 Hydrogel array fabrication schematic. **a** Schematic of stereolithographic 3D printers used to fabricate hydrogel particles. **b** Comparison of hydrogel particle diameter and spacing specified in CAD file (top view, zoom inset of digital rendering) and fabricated part (top view, zoom inset of brightfield image). **c** Quantitative comparison of PEGDA 700 g mol^{-1} hydrogel particle specified and fabricated part diameter reveals a swelling ratio of 140 %. **d** Quantitative comparison of PEGDA 700 g mol^{-1} hydrogel particle spacing

shown in Fig. 3 for 20 % and 30 % PEGDA. While the thickness of each layer is dependent on the polymer composition, a defined interface between layers can be created in both cases, as long as the polymer concentration is the same across layers.

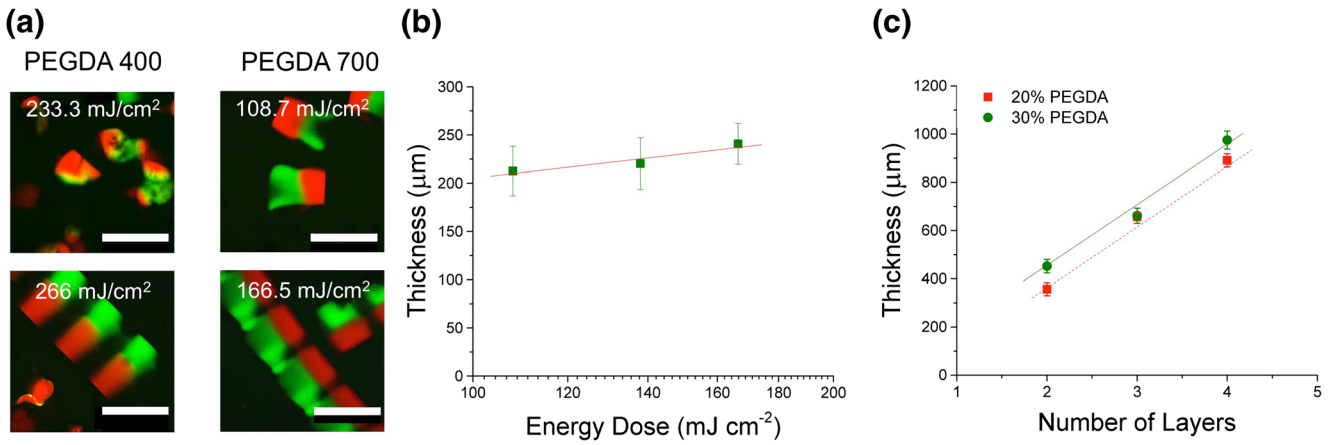

Fig. 2 Multi-material 3D fabrication. **a** Regulation of ultraviolet energy dose provides a mechanism of control over polymerization kinetics and cross-linking density, with the degree of crosslinking mediated by the composition of the polymer. Scale bars correspond to 500 μm. **b** Thickness of hydrogel particles can also be regulated by tuning the ultraviolet energy dose, with higher energy doses corresponding to larger thicknesses (note that x- axes do not start from zero values). **c** Varying the concentration of PEGDA in the pre-gel solution provides an additional mechanisms of control over particle thickness

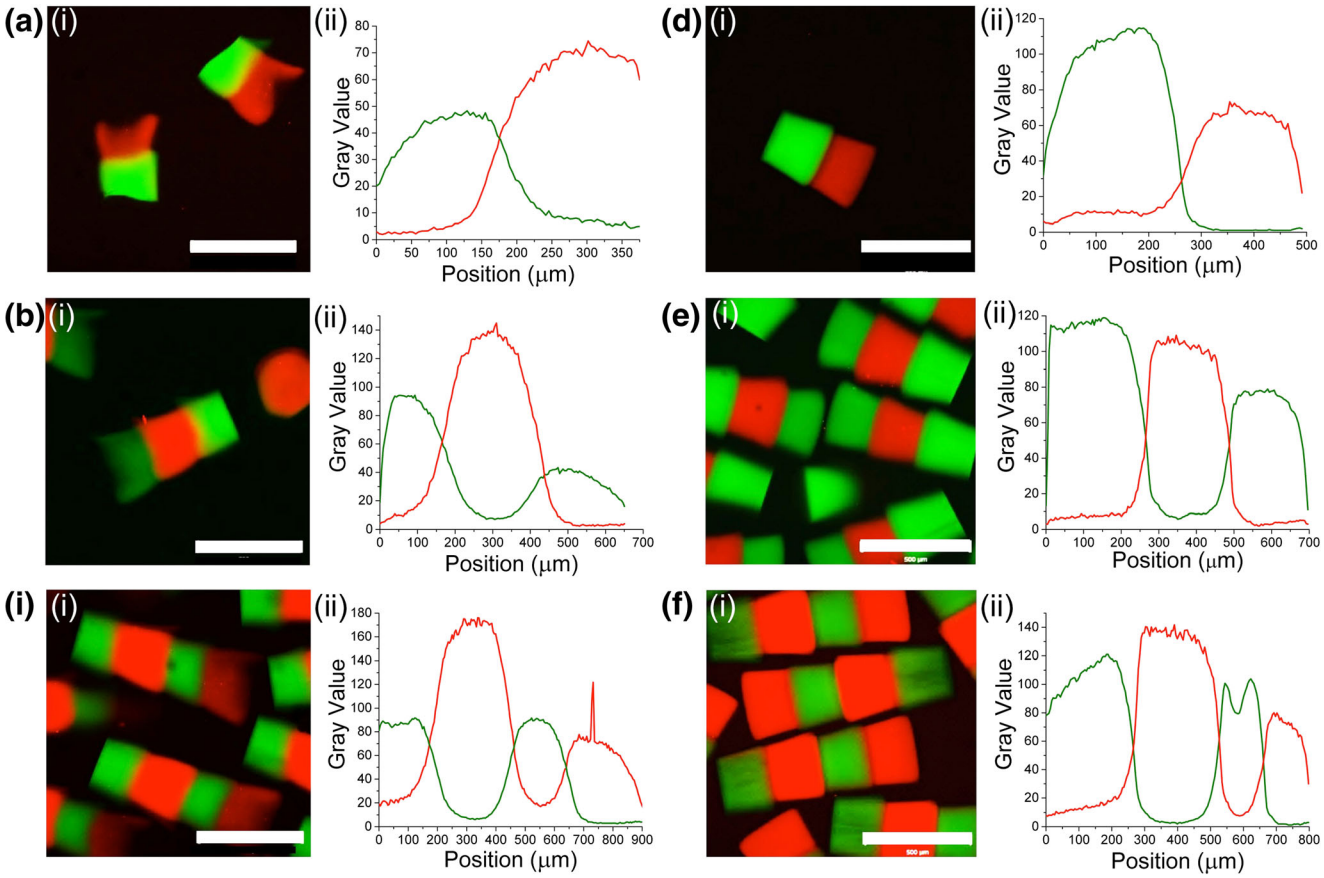

Fig. 3 Boundary stability characterization of multi-layer hydrogel particles. **a-c** Confocal images (i) and plots of light intensity/Gray value as a function of position along the thickness of a gel particle (ii) for two-layer (a), three layer (b), and four-layer (c) hydrogel particles fabricated using 20 % PEGDA 700 g mol^{-1} tagged with red or green fluorophore. Scale bars correspond to 500 μm. **d-f** Confocal images (i) and plots of light intensity/Gray value as a function of position along the thickness of a gel particle (ii) for two-layer (d), three layer (e), and four-layer (f) hydrogel particles fabricated using 30 % PEGDA 700 g mol^{-1} tagged with red or green fluorophore. Scale bars correspond to 500 μm

This boundary stability suggests that this high-throughput 3D printing approach can be used to spatio-selectively distribute different properties within a single gel particle.

2.3 Spatial compartmentalization of function epitopes in multi-layered hydrogel particles

Coupling the SLA fabrication approach with a chemical conjugation technique enabled the spatioselective localization of biomolecules within specific layers of the gels (Fig. 4). One layer of the gel particle was modified by introducing alginate methacrylate (AM), which can cross-link with PEGDA, into the pre-gel solution as shown in Fig. 4a and Fig. S2. Incorporation of fluorescent protein A, 1-ethyl-3-carbodiimide (EDC), and n-hydroxysuccinimide (NHS) into the fabricated gel containing PEGDA and AM resulted in protein A molecules chemically conjugated to AM molecules via a carbodiimide-induced chemical reaction. A stability test conducted using rhodamine-tagged protein A shows one compartment of the gel selectively conjugated with protein A (Fig. 4b). Protein A has been previously used to immobilize a variety of antibodies on different nanoparticle surfaces (Lai et al. 2015). Therefore, this chemistry and processing technique will be broadly applicable to the spatioselective biochemical modification of multi-layered gels.

To highlight the importance of spatially organizing different functional moieties in these gels, each layer of the two-layer gel particle was functionalized with superparamagnetic iron oxide nanoparticles (SPIONs) and bovine serum albumin (BSA), respectively, as shown in Fig. 4c. SPIONs are widely used as a magnetic resonance (MR) imaging contrast agent (Annabi et al. 2013; Jeong et al. 2012). By separating SPIONs from BSA, a model large molecule drug, we aimed to minimize interferential effects between SPIONs and BSA. The SPIONs would generate larger contrast in MR images, while BSA molecules would be released at controlled rates.

As shown in Fig. 4d, MR images of an agarose gel loaded with bi-layered gel particles demonstrated that particles loading BSA and SPIONs within different gel layers created a larger contrast than those in which BSA and SPIONs are encapsulated in the same layer. Using ImageJ, the average pixel

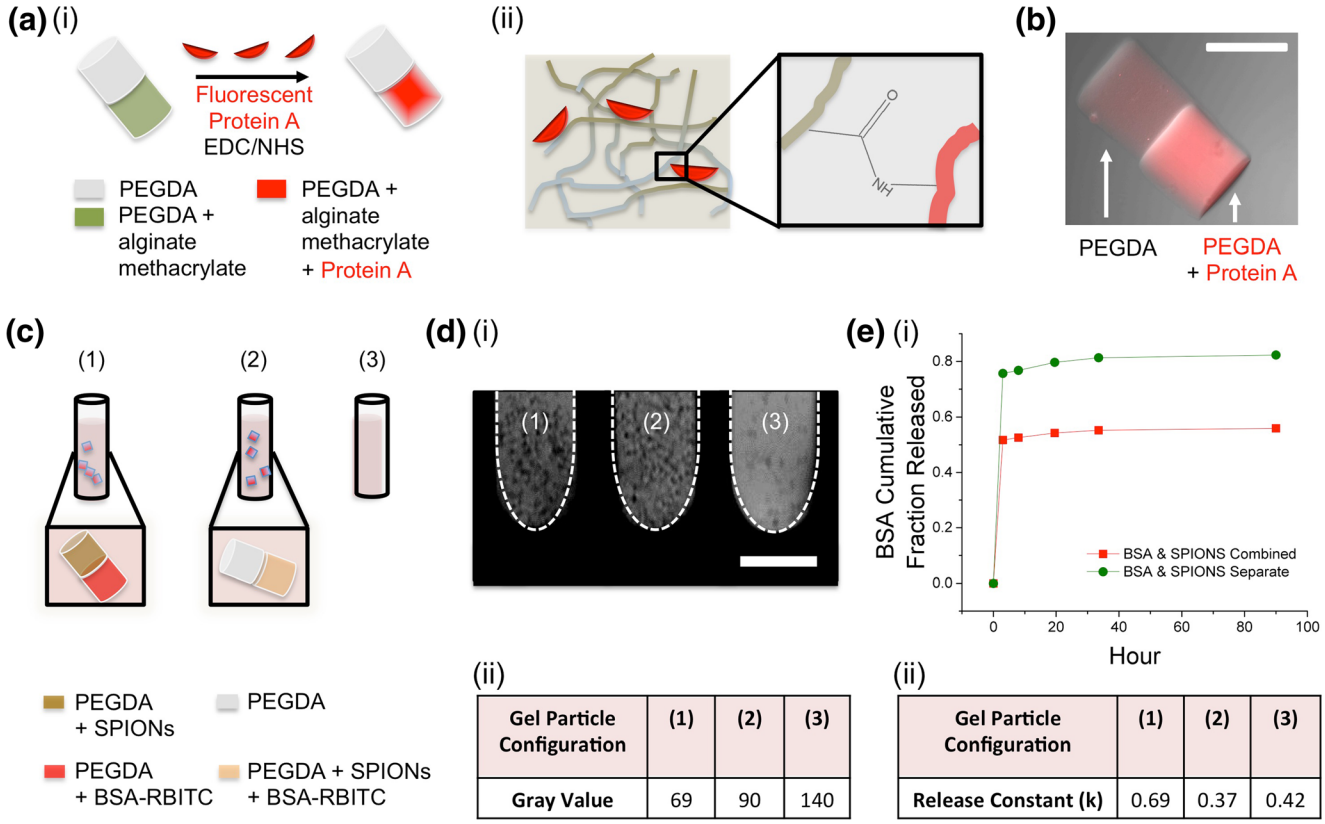

(ii)

Gel Particle Configuration	(1)	(2)	(3)
Gray Value	69	90	140

(ii)

Gel Particle Configuration	(1)	(2)	(3)
Release Constant (k)	0.69	0.37	0.42

Fig. 4 Spatioselective functionalization of hydrogel particles. **a** Schematic of chemical composition of pre-gel solutions in each layer of a two-layer particle. One layer contains pure PEGDA and the other is a mixture of PEGDA and alginate methacrylate, allowing for the fabrication of a cross-linked 3D matrix of inter-locked PEGDA and alginate monomers following UV-initiated cross-linking (i). Spatial segregation of alginate in one layer of a two-layer particle allows for spatially selective localization of fluorophore-tagged proteins (ii). **b** Spatial segregation of fluorophore-tagged protein as visualized using fluorescence imaging. Scale bar corresponds to 200 μm. **c** Schematic depicting particles loaded into an agarose gel in a glass tube for MR imaging. (1) depicts the gel particle with BSA-RBITC and SPIONs segregated, (2) depicts the gel particle with BSA-RBITC and SPIONs co-encapsulated, and (3) depicts a blank agarose gel as a control. **d** The resulting MR images (i) of (1), (2), and (3). Scale bar corresponds to 6 mm. Gray values show greater contrast in particles with phase separation (ii). **e** Cumulative fraction of encapsulated BSA released as a function of time for the separate and combined cases (i) demonstrating the enhanced release kinetics observed in biphasic particles (ii)

intensity (mean gray value) was quantified for each image captured with a spin-echo sequence. At a given echo time, an image with more contrast correlates with a darker image and a lower mean gray value. The gray value for gels with BSA and SPIONs in separate compartments indicated the highest degree of contrast, demonstrating the advantage of segregation of functional moieties within a gel.

Furthermore, measurements of the cumulative fraction of BSA released, shown in Fig. 4e, demonstrate that a significantly larger amount of BSA was released from the gels in which BSA and SPIONs were loaded in separated layers. The gels in which SPIONs and BSA were encapsulated in the same layer released only 50 % of loaded BSAs over 4 days, thus implicating the presence of uncontrolled attraction between SPIONs and BSA in the gels. By contrast, the gels with spatial segregation between SPIONs and BSA released 80 % of BSA molecules within 48 h. As determined from the Peppas-Ritger equation (Ritger and Peppas 1987), the gels with BSA and SPIONs in separate layers had a 1.9-fold larger release rate constant (k) than the gels with BSA and SPIONs in the same gel layer. Spatial segregation thus circumvented undesirable interactions between nanoparticles and proteins in the biphasic configuration.

3 Conclusions

This study demonstrates a customizable fabrication methodology for creating biphasic gel particle arrays. Stereolithographic fabrication allows for precise tuning of the gel array shape, size, and cross-linking density by providing mechanisms for precise regulation of polymerization kinetics. The properties of gels can be readily tuned to suit different applications through spatial segregation of bioactive moieties within different compartments. In future studies, multi-layered multi-functional gel constructs can be targeted at a wide variety of biomedical applications including medical diagnosis and therapeutics.

4 Experimental section

4.1 Pre-gel solution production

Poly (ethylene glycol) diacrylate (PEGDA) with molecular weights of 400 and 700 g mol^{-1} (Sigma-Aldrich) were dissolved in phosphate buffered saline (PBS, Corning CellGro) at concentrations of either 200, 250, or 300 mg mL^{-1}. Separately, 1-[4-(2-hydroxyethoxy) phenyl]-2-hydroxy-2-methyl-1-propanone-1-one photoinitiator (Irgacure 2959, Ciba Chemicals) was dissolved in dimethyl sulfoxide (DMSO, Fisher Scientific), and mixed with the PEGDA solution to reach a final concentration of 1–5 mg mL^{-1} Irgacure 2959. Alginate methacrylate (AM)/PEGDA pre-gel solution, a mass of PEGDA was weighed, dissolved in the presence of 5 mg mL^{-1} AM in PBS, and degassed under vacuum in the dark for at least 12 h. AM was prepared by conjugating 2-aminoethylmethacrylate to the carboxylic acids of alginate (FMC) via carbodiimide chemistry, as previously reported (Cha et al. 2009). Bovine serum albumin (BSA, Sigma-Aldrich) was functionalized with either fluorescein-isothiocyanate or rhodamine B-isothiocyanate to form BSA-FITC or BSA-RBITC, respectively.

4.2 Stereolithographic 3D printing

CAD software (SolidWorks, Dassault Systems) was used to fabricate arrays of particles of varied dimensions and spacing. These were manufactured using a laser-based stereolithographic apparatus (SLA 250/50, 3D Systems). As the laser (325 nm) rasterized across the surface of the pre-gel solution in the pattern prescribed by the CAD file, it was cross-linked or "cured" in regions that were exposed to ultraviolet light. Following fabrication of each layer of the array, the motorized SLA stage moved down by a prescribed amount and the rasterizing process was repeated. Once the multi-layer array was complete, the particles were washed and stored in PBS and kept in the dark at 4°C until imaging.

4.3 Confocal imaging

After fabrication, particles were gently detached from the glass slide using a plastic Pasteur pipette, placed in a dish, and imaged using a confocal microscope (Zeiss LSM 700, objectives: 10X/0.3 or 20X/0.8). The excitation wavelength was either 488 nm (for BSA-FITC) or 555 nm (for BSA-RBITC). As needed, brightfield images were captured in parallel with fluorescent images. All image analysis was done with ImageJ software (NIH) or Zen 2 Lite (Zeiss).

4.4 Modification of particles with fluorescent *Staphylococcus aureus* protein A (SpA)

SpA was modified with RBITC, as previously described (Lai et al. 2015). Particles were incubated in 7 mg mL^{-1} of 1-ethyl-3-carbodiimide (EDC) and 10 mg mL^{-1} of n-hydroxysuccinimide (NHS) for 30 min. The particles were then washed, and a small volume of 2-mercaptoethanol was added. They were then incubated in 1 mg mL^{-1} SpA-RBITC (protein A-RBITC) for 15 min, washed 5 times, and imaged.

4.5 Magnetic resonance imaging

Particles were fabricated with PEGDA containing superparamagnetic iron oxide nanoparticles (SPIONs, SHP-10-10; Ocean NanoTech) and BSA-RBITC. BSA-RBITC and SPION concentration were constant at 1 mg mL^{-1} and 100 μg Fe mL^{-1}, respectively. After fabrication, particles were dispersed in PBS, then rapidly mixed with warm 10 mg mL^{-1} agarose solution in a borosilicate tube and gelled at room temperature. An agarose gel with no particles was prepared as a control. MR images were captured with a spin-echo sequence on a Varian 600 MHz Small-Bore Scanner.

4.6 Quantification of BSA release

After fabrication, particles were released, mixed in PBS, then incubated at 37 °C and shaken at 100 rpm (Heidolph Rotamax 120). At each time-point, the particles were centrifuged at 100 rcf for 3 min (Eppendorf centrifuge 5424). The fluorescent intensity of the supernatant was then measured (Tecan Infinite 200 PRO). The total theoretical amount of BSA-RBITC encapsulated was estimated by considering the volume of a rod-shaped particle with a diameter of 250 μm and a height of 250 μm loaded with 1 mg mL^{-1} of BSA. BSA release rate was quantified according to the Peppas-Ritger equation: $M_t/M_\infty = (k)(t^n)$, where M_t is the mass released at time t, M_∞ corresponds to the mass released at time infinity (total amount encapsulated), and k and n correspond to the release constant and the diffusional exponent, respectively.

Acknowledgments We acknowledge Boris Odintsov for his assistance in MR imaging. This work was funded by the National Science Foundation (NSF) Science and Technology Center EBICS (Grant CBET-0939511) and National Institute of Health (1R01 HL109192 to H.K). R.R was funded by an NSF Graduate Research Fellowship (Grant DGE-1144245) and NSF CMMB IGERT at UIUC (Grant 0965918). N.C. was funded by a Dow Graduate Fellowship.

References

Annabi, N. et al., 2013. 25th Anniversary Article: Rational Design and Applications of Hydrogels in Regenerative Medicine. *Advanced Materials*, p.n/a–n/a. Available at: http://doi.wiley.com/10.1002/adma.201303233 [Accessed November 8, 2013].

Arcaute, K., Mann, B.K. & Wicker, R.B., 2011. Practical use of hydrogels in stereolithography for tissue engineering applications. In P. J. Bártolo, ed. *Stereolithography*: *Materials*, *Processes*, *and Applications*. Boston, MA: Springer US, pp. 299–331. Available at: http://link.springer.com/10.1007/978-0-387-92904-0 [Accessed February 21, 2014].

Bartolo, P.J., 2011. Stereolithographic processes. In P. J. Bártolo, ed. *Stereolithography*: *Materials*, *Processes and Applications*. Boston, MA: Springer US, pp. 1–36. Available at: http://www.springerlink.com/index/10.1007/978-0-387-92904-0 [Accessed February 16, 2013].

S. Bhaskar et al., Towards designer Microparticles: simultaneous control of anisotropy, shape, and size. Small **6**(3), 404–411 (2010)

C. Cha, R. H. Kohman, H. Kong, Biodegradable polymer Crosslinker: independent control of stiffness, toughness, and hydrogel degradation rate. Adv. Funct. Mater. **19**(19), 3056–3062 (2009). http://doi.wiley.com/10.1002/adfm.200900865 [Accessed July 1, 2014] Available at:

Chan, V. et al., 2010. Three-dimensional photopatterning of hydrogels using stereolithography for long-term cell encapsulation. Lab Chip, 10(16), pp. 2062–2070. Available at: http://www.ncbi.nlm.nih.gov/pubmed/20603661 [Accessed February 12, 2013].

Jeong, J.H. et al., 2012. "Living" microvascular stamp for patterning of functional neovessels; Orchestrated control of matrix property and geometry. Adv. Mater., 24(1), pp. 58–63, 1. Available at: http://www.ncbi.nlm.nih.gov/pubmed/22109941 [Accessed February 11, 2013].

M. Lai et al., Bacteria-mimicking nanoparticle surface functionalization with targeting motifs. Nanoscale **7**, 6737–6744 (2015)

B. Li et al., Multifunctional hydrogel Microparticles by polymer-assisted photolithography. *ACS Appl. Mater. Interfaces* **8**, 4158–4164 (2016)

Melchels, F.P.W., Feijen, J. & Grijpma, D.W., 2010. A review on stereolithography and its applications in biomedical engineering. *Biomaterials*, 31(24), pp. 6121–6130. Available at: http://www.ncbi.nlm.nih.gov/pubmed/20478613 [Accessed November 18, 2013].

J. A. S. Neiman et al., Photopatterning of hydrogel scaffolds coupled to filter materials using stereolithography for perfused 3D culture of hepatocytes. Biotechnol. Bioeng. **112**(4), 777–787 (2015). http://doi.wiley.com/10.1002/bit.25494Available at:

N. A. Peppas et al., Hydrogels in biology and medicine: from molecular principles to Bionanotechnology. Adv. Mater. **18**(11), 1345–1360 (2006). http://doi.wiley.com/10.1002/adma.200501612 [Accessed September 22, 2013]Available at:

Raman, R. et al., 2015. High-Resolution Projection Microstereolithography for Patterning of Neovasculature. *Advanced Healthcare Materials*, pp. 1–10.

R. Raman, R. Bashir, Stereolithographic 3D Bioprinting for Biomedical Applications. In *Essentials 3D Biofabrication Transl*, 89–121 (2015)

P. L. Ritger, N. A. Peppas, A simple equation for description of solute release. J. Control. Release **5**, 23–36 (1987)

K. Roh, D. C. Martin, J. Lahann, Biphasic Janus particles with nanoscale anisotropy. Nat. Mater. **4**, 759–763 (2005)

B. R. K. Shah, J. Kim, D. A. Weitz, Janus Supraparticles by induced phase separation of nanoparticles in droplets. Adv. Mater. **729**, 1949–1953 (2009)

E. V. Shevchenko et al., Gold/iron oxide core/hollow-shell nanoparticles. Adv. Mater. **20**(22), 4323–4329 (2008)

Stampfl, J. & Liska, R., 2011. Polymerizable hydrogels for rapid prototyping: chemistry, photolithography, and mechanical properties. In P. J. Bártolo, ed. *Stereolithography*: *Materials*, *Processes and Applications*. Boston, MA: Springer US. Available at: http://www.springerlink.com/index/10.1007/978-0-387-92904-0 [Accessed February 16, 2013].

S. Yang et al., Microfluidic synthesis of multifunctional Janus particles for biomedical applications. Lab Chip **12**(12), 2097 (2012)